

Bai Shichen (Orcid ID: 0000-0001-8937-7987)
Shi Quanqi (Orcid ID: 0000-0001-6835-4751)
Liu Terry Zixu (Orcid ID: 0000-0003-1778-4289)
Zhang Hui (Orcid ID: 0000-0001-5346-7112)
Yue Chao (Orcid ID: 0000-0001-9720-5210)
Sun Wei-Jie (Orcid ID: 0000-0001-5260-658X)
Tian Anmin (Orcid ID: 0000-0002-4351-551X)
Degeling Alexander William (Orcid ID: 0000-0001-7338-9270)
Bortnik Jacob (Orcid ID: 0000-0001-8811-8836)
Rae I. Jonathan (Orcid ID: 0000-0002-2637-4786)
Wang Mengmeng (Orcid ID: 0000-0002-7686-1910)

Ion Scale Flux Rope Observed Inside a Hot Flow Anomaly

Shi-Chen Bai^{1,2}, Quanqi Shi¹, Terry Z. Liu^{3,4,5}, Hui Zhang⁵, Chao Yue^{2,6}, Wei-Jie Sun⁷
Anmin Tian¹, Alexander W. Degeling¹, Jacob Bortnik², I. Jonathan Rae⁸,
Mengmeng Wang¹

¹Shandong Provincial Key Laboratory of Optical Astronomy and Solar-Terrestrial Environment, School of Space Science and Physics, Shandong University, Weihai, China.

²Department of Atmospheric and Oceanic Sciences, University of California, Los Angeles, California, CA, USA.

³University Corporation for Atmospheric Research, Boulder, CO, USA

⁴Department of Earth, Planetary, and Space Sciences, University of California, Los Angeles, California

⁵Geophysical Institute, University of Alaska Fairbanks, Alaska, USA

⁶Institute of Space Physics and Applied Technology, Peking University, Beijing, China

⁷Department of Climate and Space Sciences and Engineering, University of Michigan, Ann Arbor, MI, USA

This is the author manuscript accepted for publication and has undergone full peer review but has not been through the copyediting, typesetting, pagination and proofreading process, which may lead to differences between this version and the Version of Record. Please cite this article as doi: [10.1029/2019GL085933](https://doi.org/10.1029/2019GL085933)

⁸Mullard Space Science Laboratory, Space and Climate Physics, University College
London, Dorking, UK

Author Manuscript

Abstract

We report an earthward moving ion scale flux rope embedded within the trailing edge of a hot flow anomaly (HFA) observed by the Magnetospheric Multiscale (MMS) satellite constellation on 17 December 2016 upstream of Earth's quasi-parallel bow shock. The driver of the HFA, a tangential discontinuity, was observed by the Wind spacecraft without flux rope signatures around it in the solar wind. This suggests that the earthward moving flux rope was generated inside the HFA. This ion scale flux rope is not a force free structure and expands due to a strong magnetic pressure gradient force. Solar wind ions are decelerated inside the flux rope by the static electric field likely caused by the charge separation of solar wind particles. Our observations imply that magnetic reconnection may have occurred inside the HFA. Reconnection and flux ropes may play a role in particle acceleration/heating inside foreshock transients.

Key Points:

1. An ion scale flux rope with 6.1-7.5 ion inertial length is observed at the trailing edge of a hot flow anomaly.
2. Solar wind ions were decelerated inside the flux rope and the kinetic energy of solar wind ions was likely converted to the magnetic energy.
3. The flux rope is close to a one-dimensional structure and expands due to the strong magnetic pressure gradient force.

Plain Language Summary

Energetic particles are often observed inside the foreshock transients or in the foreshock region. The acceleration mechanisms of these energetic particles remain an open question. Possible candidates responsible for the acceleration have been put forward, such as Fermi acceleration, electron firehose and lower hybrid drift instabilities and magnetic reconnection. However, to date magnetic reconnection is only found in hybrid simulations during the generation of foreshock transients, but never reported by in-situ observations. In this paper, we report an ion scale flux rope observed at the trailing edge of a hot flow anomaly, which could be generated during the magnetic reconnection. Our observations indicate that reconnection could occur locally within foreshock transients and contribute to their particle acceleration.

1. Introduction

Hot flow anomalies (HFAs) are frequently observed near Earth's bow shock, which are characterized by a superheated, tenuous, low-field-strength core region [Schwartz *et al.*, 1985; Schwartz *et al.*, 2000; Zhang *et al.*, 2010; Chu *et al.*, 2017; Wang *et al.*, 2013a, b, c; Zhao *et al.*, 2015, 2017]. The streaming energy of the solar wind ion beams and reflected ion beams is converted into the thermal energy inside HFAs, which leads to the expansion of HFAs. Because of the expansion, a strong deflection of the plasma velocity is exhibited within the structure, and the magnetic field and plasma compression regions or secondary shock is presented on one or both sides of the core [Thomsen *et al.*, 1988, Omidi and Sibeck 2007; Zhang *et al.*, 2010].

Energetic particles up to hundreds of keV have been observed inside the cores of foreshock transients and most of foreshock transients can accelerate/heat particles [Wilson *et al.*, 2016; Liu *et al.*, 2017a], which raises the question of how particles are accelerated and heated inside the structure. The Fermi acceleration through particle bouncing between the bow shock and the earthward moving boundary of foreshock transients is one possible candidate, which has been carefully investigated recently

[Liu *et al.*, 2017b, 2018; Turner *et al.*, 2018]. Recent observations also showed that the betatron acceleration can explain hundreds of keV electrons inside foreshock transients [Liu *et al.*, 2019]. The electron firehose and lower hybrid drift instabilities are also possible candidates for the isotropization and heating processes within HFAs [Eastwood *et al.* 2008; Zhang *et al.* 2010]. Magnetic reconnection during the development of HFA might be another possible mechanism for the particle acceleration inside HFAs [Lin, 1997]. A particle-in-cell(PIC) simulation shows that suprathermal electrons were accelerated by the magnetic islands generated by magnetic reconnection in the quasi-perpendicular shock [Matsumoto *et al.*, 2015]. Reconnection is also shown to occur in the quasi-parallel shock transition region through the Weibel instability [Gingell *et al.*, 2017]. If magnetic reconnection occurs inside foreshock transients, Fermi acceleration during the coalescence of magnetic islands could be another potential mechanism.

Recently, features of current sheet structures consistent with magnetic reconnection were found in the transition region of a quasi-parallel shock [Gingell *et al.*, 2019; Hamrin *et al.*, 2019] and quasi-perpendicular shock [Wang *et al.*, 2019] with MMS high cadence plasma measurements. Signatures of magnetic reconnection such as small-scale flux ropes, which formed due to the tearing mode instability [Daughton *et al.*, 2006; Drake *et al.*, 2006a] or electron Kelvin-Helmholtz instability [Fermo *et al.*, 2012] during the reconnection, might be found inside foreshock transients. To date only a magnetic flux rope event in the magnetosheath part of an HFA has been reported [Hasegawa *et al.*, 2012], which probably originate from magnetic reconnection in the magnetosheath part of the HFA. However, there is no clear observation of flux ropes formed locally inside foreshock transients.

In this study, we report an ion-scale flux rope observed at the trailing edge of an HFA in the ion foreshock. which is expanding and moving earthward with the HFA. The paper is organized as follows. In section 2.1, we introduce the data used in this study. In section 2.2, an overview of the HFA observed by MMS is given, in which

the ion-scale flux rope is encountered. The solar wind condition observed by ACE and Wind is also provided in this section. Detailed analysis of the flux rope embedded in the HFA is presented in section 2.3. The expansion of the flux rope is investigated in section 2.4. Section 3 briefly discusses the mechanism of the expansion of the ion-scale flux rope and the energy transfer around the flux rope.

2. Observations

2.1 Data

In this paper, the solar wind magnetic field is measured by the magnetometer onboard the Wind satellite [Lepping *et al.*, 1995] and ACE satellite [Smith *et al.*, 1998]. The foreshock observation comes from the fluxgate magnetometer (FGM; Russell *et al.*, 2016), the fast plasma investigation (FPI; Pollock *et al.*, 2016) and the electric field double probes (EDP; Lindqvist *et al.*, 2016; Ergun *et al.*, 2014) onboard the MMS satellite constellation [Burch *et al.*, 2016].

2.2 MMS Observation of an HFA

The time scale of the observed hot flow anomaly (HFA) is only 16 seconds, extending from 12:55:12 UT to 12:55:28 UT, located upstream of a quasi-parallel shock ($\theta_{Bn}=43^\circ$, determined by using the bow shock model [Slavin and Holzer 1981]) shown in the black dashed box in Figure 1. The magnitude of the magnetic field and the electron density increased at both edges and decreased in the core region of the HFA (Figures 1a and 1b), which is caused by the expansion of the HFA [Thomsen *et al.*, 1988, Omidi and Sibeck 2007]. The electron temperature increases continuously inside the HFA (Figure 1c), this might be related to the earthward motion of the HFA and the Fermi acceleration of electrons [Liu *et al.*, 2017b]. The electron velocity decreases inside the HFA (Figure 1d). Energetic foreshock ions (Figure 1e) get

thermalized inside the HFA, which provides the energy for the expansion of the HFA [Onsager *et al.*, 1990]. All of these are typical observational features of HFAs. The HFA was expanding and moving toward the bow shock based on timing analysis [Schwartz 1998]. The velocities of the leading and trailing edges of the HFA are $165.8 \pm 7.6 \times [-0.96 \ 0.01 \ 0.24]$ km/s and $91.9 \pm 3.6 \times [-0.90, -0.29 \ -0.31]$ km/s in GSM coordinates, respectively.

The prevailing solar wind parameters, observed by ACE and Wind, are shifted to the MMS location (Figures 1g and 1h). Because of the large disturbance in the magnetic field, the comparison of cone/clock angle between MMS and Wind/ACE was not used when MMS was in the foreshock region and not shown in Figures 1i-j. Using only the time interval when MMS was in the solar wind before and after the event, the comparison of the cone angle and clock angle of the interplanetary magnetic field (IMF) observed by ACE, Wind and MMS are shown in Figures 1i and 1j and the lag time between ACE/Wind and MMS is determined by the highest correlation coefficient of the cone angle ($r > 0.9$). Within this time interval, there is only one possible discontinuity observed by Wind at ~12:55:04 UT (blue shaded region; only a weak variation is observed by ACE) that might trigger the generation of the HFA. It is a tangential discontinuity (TD) identified by a near-zero normal component and a discontinuity in the tangential component of the magnetic field around it. The normal of the TD is $[-0.543, -0.830, 0.122]$ in GSM coordinates determined by the minimum variance analysis [Sonnerup & Cahill, 1967] (MVAB) and a similar normal is obtained through the cross product method [Schwartz, 1998] at Wind. The propagation of the tangential discontinuity (TD) is consistent with the time delay from Wind to MMS. The motional electric field ($E = -V \times B$) points toward the TD on both sides, consistent with the preferred condition for the HFA generation [Thomsen *et al.*, 1993]. During the entire time interval around the discontinuity no flux rope signature, such as the unipolar component and bipolar component of magnetic field is shown. A schematic illustration of the TD, the HFA, and the relative trajectory of MMS is shown in Figure 1k.

2.3 Ion Scale Flux Rope

At the trailing edge of the HFA (Figures 1-3 shaded region; 12:55:23 UT to 12:55:28 UT), the magnetic field strength and the electron density enhancement at the trailing edge are very significant. The electron density increased from 11.35 cm^{-3} in the solar wind to 80.98 cm^{-3} at the trailing edge of the HFA and the magnetic field strength also increased from 4.5 nT in the solar wind to 34.0 nT at the trailing edge of the HFA with a compression ratio much larger than 4. This means that it is not a typical compressional boundary. The bipolar B_z and unipolar B_y suggest that it could be a small-scale flux rope. Using the timing analysis [Schwartz, 1998], the velocities of the leading and trailing edges of the flux rope are $113.5 \pm 5.9 \times [-0.84, -0.32, -0.43]$ km/s and $91.93 \pm 3.6 \times [-0.90, -0.29, -0.31]$ km/s in GSM coordinate, respectively. This suggests that the flux rope is expanding at ~ 20 km/s toward the sun in the solar wind reference frame. The spatial scale of the flux rope is 6.10-7.51 ion inertial lengths. The ion inertial length here is 75.5 km determined by the ion density in the solar wind (12:55:30-12:55:40 UT). The expansion of the flux rope will be carefully investigated in the next section.

To better investigate this case, we use the L-M-N coordinate system, which is determined by MVAB [Sonnerup & Cahill, 1967]. We found that $L \sim [-0.18, 0.98, -0.07]$, $M \sim [-0.46, -0.02, 0.88]$ $N \sim [0.86, 0.19, 0.45]$ are the maximum, intermediate and minimum variation directions in GSM coordinates respectively. The core field of the flux rope is in the L direction and the bipolar signature is shown in the M direction. B_N is negative and decreased inside the flux rope. Field-aligned current which is calculated using the culometer technique [Dunlop *et al.*, 1988, 2002] was observed at the center of the flux rope (Figure 2b). Due to the presence of helical structure inside the flux rope, the local radius of curvature of the magnetic field lines increases from 300 to 1000 km inside the flux rope (Figure 2c), which is obtained by magnetic field rotation analysis [Shen *et al.*, 2007]. The observational features of the magnetic field,

current density and radius of curvature of the magnetic field lines listed above are consistent with the previous work on flux ropes [e.g., *Russell and Elphic* 1979; *Slavin et al.*, 2003; *Shen et al.*, 2007; *Zong et al.*, 2004; *Sun et al.*, 2019].

The electric field is shown in Figure 2d and we focus on the component in the normal direction. Two ion populations were observed inside the flux rope, one comes from the solar wind from 10 to 1000 eV and the other from the foreshock ions from 1keV to 3keV (see Figure 1e). The $\mathbf{V} \times \mathbf{B}$ of these two ion populations are quite different. The $\mathbf{V}_{i_solarwind} \times \mathbf{B}$ agrees well with the $\mathbf{V}_e \times \mathbf{B}$. For foreshock ions, on the other hand, the $\mathbf{V}_{i_foreshock} \times \mathbf{B}$ does not match the $\mathbf{V}_e \times \mathbf{B}$ at all. There is also disagreement between the $\mathbf{V}_e \times \mathbf{B}$ and the electric field measured by EDP from 12:55:26 to 12:55:27.5 UT. One possible reason is that when the solar wind penetrates the flux rope, the gyroradii difference between the solar wind ions and electrons generates the electrostatic field in normal direction which could decelerate the solar wind ions. Considering the velocity of the trailing edge of the HFA, the spatial scale of this disagreement electric field is 133.56 km, which is close to the gyroradii difference between the solar wind ions and electrons (142.03 km for 1 keV solar wind particles). To further confirm this, we calculated this static electric field in +N direction through the disagreement between EDP measurement and $\mathbf{V}_e \times \mathbf{B}$ and compared it with the energy decrease of solar wind ions. Here we used the average value of the disagreement between the $\mathbf{V}_e \times \mathbf{B}$ and the measured electric field from 12:55:26 to 12:55:27.5 UT as the static electric field $E=1.7\text{mV/m}$. Then we calculated the solar wind energy decrease as $1.7 \text{ mV/m} \cdot 133.56 \text{ km}$ in the de Hoffmann Teller frame [*Sonnerup et al.*, 1987] ($V_{HT}=232.5 \times [-0.96, 0.28, 0.07] \text{ km/s}$) and transformed it back to the spacecraft frame shown as the white solid lines in Figure 2g. It matches the energy where the solar wind ion flux peaks very well, confirming the deceleration of solar wind ions by the static electric field at the trailing edge of flux rope. There is no significant change in the T_{para} of the solar wind ions around the trailing edge of the flux rope (red in Figure 2f). The T_{perp} (blue in Figure 2f), on the other hand, increases during the deceleration of solar wind ions at the boundary of the flux rope

possibly due to the magnetic field strength enhancement. At the peak of the field strength where J_L reaches the peak, however, the perpendicular temperature decreases, and the parallel motion dominates (Figure 2h). This is again inconsistent with typical compressional boundaries or shocks, but more consistent with field-aligned particle motion inside flux ropes.

To see it more clearly, Figure 2i shows the ion distribution at 12:55:25.24 UT (marked by the vertical dashed line) when the field-aligned current peaked. The white dashed and solid line overlaid in Figure 2i represent the ions with the same parallel velocity, suggesting that the solar wind ions are decelerated and thermalized in the perpendicular plane inside the flux rope than in the solar wind. Figure 2i shows the ion distribution in the M-N plane (roughly the plane perpendicular to the magnetic field as B_L dominates), the $E \times B$ motion of the solar wind ions is mainly in the M direction and the thermalization of the solar wind ions are mainly in the N direction. The red dashed line in Figure 2j is the velocity of trailing edge of the flux rope in the normal direction. Most of the solar wind ions are faster than that speed (V_n).

2.4 Force Analysis Inside the Flux Rope

To understand why the structure is expanding, Figure 3 shows the pressure and force analysis inside the flux rope. Because the spatial scale of the flux rope is too small compared to the gyroradii (~ 710 km) of foreshock ions and the foreshock ion density is much lower than the solar wind ion density, we ignore the pressure and pressure gradient force caused by the foreshock ions inside the flux rope and separate the solar wind ions (10-1000eV) from the total ion distribution. However, foreshock ions still contribute to the current and electrostatic field inside the flux rope. Before we analyze each term on the right side of the MHD momentum equation (Eq. 1), we test the reliability of our calculation by comparing the sum of the ion density calculated by two ion populations with the MMS measurement (Figure 3b), which

shows excellent agreement.

As shown in Figure 3c, the magnetic pressure is enhanced at the center of the flux rope and the thermal pressure reaches the two peaks at two edges of the flux rope. Each term on the right side of the momentum equation shown below is calculated in L-M-N coordinates and displayed in Figures 3d-f. The pressure gradients are calculated based on the pressure tensor.

$$\rho \left(\frac{\partial}{\partial t} + \vec{\mathbf{V}} \cdot \nabla \right) \vec{\mathbf{V}} = -\nabla_{\perp} \left(\frac{\mathbf{B}^2}{2\mu_0} \right) + \frac{\mathbf{B}^2}{\mu_0} (\vec{\mathbf{b}} \cdot \nabla) \vec{\mathbf{b}} - \nabla \cdot \vec{\mathbf{P}} \quad (1)$$

In the L direction (Figure 3d), the ion pressure gradient determines the motion of the flux rope, whereas the other three terms are insignificant inside the flux rope. In the M direction, the motion of the flux rope is determined by the magnetic pressure gradient and ion pressure gradient force. The M component of the magnetic pressure gradient and magnetic tension force (Figure 3e) changes direction during the MMS crossing, indicating that the MMS is crossing the center of the flux rope rather than a pressure pulse driven structure, otherwise the M component should be unidirectional [Sibeck *et al.*, 1990; Lockwood, 1991]. In the N direction (Figure 3f), the magnitude of the magnetic pressure gradient force is much larger than the other two terms and determines the expansion of the flux rope. Magnetic tension force in the normal direction is very weak inside the flux rope, which suggests that the field line might be elongated in the M direction rather than circular in the M-N plane. Another piece of evidence to support this point is that the dimension of this flux rope is quasi-one-dimensional (1D) rather than two-dimensional (2D) structure as usual which is determined by the Minimum Directional Derivative (MDD) method [Shi *et al.*, 2005, Shi *et al.*, 2019]. The structure should be 1D when $\sqrt{\lambda_{max}} \gg \sqrt{\lambda_{mid}}$, $\sqrt{\lambda_{min}}$ as shown in Figure 3g. λ_{max} , λ_{mid} and λ_{min} are three eigenvalues of a symmetrical matrix $L = GG^T = (\nabla \vec{\mathbf{B}})(\nabla \vec{\mathbf{B}})^T$, which represent the maximum,

intermediate and minimum values of the field directional derivatives, respectively.

3. Summary and Discussion

In this paper, we report a small-scale flux rope with the width of 6.1-7.5 ion inertial lengths at the trailing edge of the HFA in the foreshock for the first time, which is characterized by the bipolar signature of the B_M component, a strong core field, and field aligned current. Inside the flux rope, the perpendicular temperature decreased, and the M components of the magnetic gradient force changes direction several times. Both features further support that it is a flux rope, rather than a typical compressional boundary at the trailing edge of the HFA. A tangential discontinuity was observed in the solar wind which may leads to the generation of the HFA. However, no flux rope signature was observed in the solar wind around the discontinuity and the flux rope is moving toward the bow shock, indicating that the ion-scale flux rope is locally generated at the trailing edge of the HFA, rather than being generated in the magnetosheath or in the solar wind and propagating to the core region of the HFA.

Solar wind ions are decelerated at the boundary of the flux rope between 12:55:26 and 12:55:28 UT, which is related to the positive static E_N pointing towards the solar wind possibly caused by the charge separation of the solar wind particles. The perpendicular temperature of solar wind ions (10-1000 eV) increased simultaneously, indicating that solar wind ions at the HFA boundary are strongly diffused in the normal direction, and the kinetic energy of solar wind ions is converted into the thermal energy. Inside the flux rope, however, the parallel ion motion dominates. These parallel motion-dominated solar wind ions could be decelerated by the -L electric field and eventually trapped inside the flux rope, which may lead to the unusual high density observed by MMS. There is no enhancement of the thermal energy inside the flux rope. Instead, the perpendicular temperature decreases although the magnetic field strength continues to increase. The kinetic energy of solar wind

ions was probably converted to the magnetic energy with the local $\mathbf{J} \cdot \mathbf{E}'$ in the flux rope close to -0.9 nW/m^3 . These features further indicate that the trailing edge of the HFA is not a typical compressional boundary or shock, but a flux rope.

The M component of the magnetic pressure gradient and magnetic tension changes directions several times during the flux rope crossing, indicating that the MMS crosses the center of the flux rope. The N component of the magnetic tension force is close to zero, indicating that the flux rope is a quasi-1D structure which is easier to be observed in the magnetic reconnection with small guide field than quasi-2D flux rope [Sun *et al.*, 2019]. This transient quasi-1D flux rope is not a force free structure and expanding mainly in the normal direction, which is determined by the magnetic pressure gradient force. Therefore, reconnection might be triggered within the HFA at the early stage during the interaction between the discontinuity and the bow shock, which is consistent with the hybrid simulation [Lin, 1997] and MMS observation [Hamrin *et al.*, 2019]. Additionally, this provides another way to generate energetic electrons inside foreshock transients that electrons could be accelerated up to hundreds of keV during the coalescence of ion-scale flux ropes [Drake *et al.*, 2006b; Matsumoto *et al.*, 2015]. However, electrons with hundreds of keV were not observed in this case, which might have not been generated yet or have leaked to the foreshock region like energetic ions [Liu *et al.*, 2017c]. Our observations of the ion-scale flux rope inside the HFA fills in the blank of in-situ observation of reconnection signature inside foreshock transients and might shed light on the particle acceleration in the foreshock region.

4. Acknowledgement

MMS data are available at MMS Science Data Center (<https://lasp.colorado.edu/mms/sdc/>). This work was supported by the National Natural Science Foundation of China (grants 41574157, 41774153, 41731068 and 41961130382), Project Supported by the Specialized Research Fund for State Key Laboratories, International Space Science Institute (ISSI), and the young scholar plan of Shandong University at Weihai (2017WHWLJH08). S.-C. B. is supported by the State Scholarship Fund of Chinese Scholarship Council. I. J. R. is funded in part by STFC grant ST/N0007722/1 and Natural Environment Research Council (NERC) grants NE/L007495/1, NE/P017150/1, and NE/P017185/1. T. Z. L. is supported by the NASA Living With a Star Jack Eddy Postdoctoral Fellowship Program, administered by the Cooperative Programs for the Advancement of Earth System Science (CPAESS). H. Z. is partially supported by NSF AGS-1352669. J. B. is supported by NNX14AI18G.

5. Reference

Burch, J. L., T. E. Moore, R. B. Torbert, and B. L. Giles (2016), Magnetospheric multiscale overview and science objectives, *Space Sci. Rev.*, 199, 5–21, doi:10.1007/s11214-015-0164-9.

Chu, C. S., H. Zhang, D. G. Sibeck, Otto, A., Zong, Q., Omidi, N., McFadden, J. P., Fruehauff, D., and Angelopoulos, V. (2017), THEMIS satellite observations of hot flow anomalies at Earth's bow shock, *Ann. Geophys.*, 35, 443-451, doi:10.5194/angeo-35-443-2017.

Daughton, W., J., Scudder and H. Karimabadi, (2006). Fully kinetic simulations of undriven magnetic reconnection with open boundary conditions. *Physics of Plasmas*, 13(7), 072101.
<https://doi.org/10.1063/1.2218817>

Denton, R. E., et al. (2018), Determining L-M-N Current Sheet Coordinates at the Magnetopause From Magnetospheric Multiscale Data, *Journal of Geophysical Research: Space Physics*, 123(3), 2274-2295, doi:10.1002/2017JA024619.

Drake, J. F., M. Swisdak, K. M. Schoeffler, B. N. Rogers and S. Kobayashi, (2006a). Formation of secondary islands during magnetic reconnection. *Geophysical Research Letters*, 33, L13105.
<https://doi.org/10.1029/2006GL025957>

Drake, J. F., M. Swisdak, H. Che and M. A. Shay (2006b), Electron acceleration from contracting magnetic islands during reconnection, *Nature*, 443, 553, doi:10.1038/nature05116

Dunlop, M. W., A. Balogh, K.-H. Glassmeier and P. Robert (2002), Four-point Cluster application

of magnetic field analysis tools: The Curlometer, *J. Geophys. Res.*, 107(A11), 1384,
doi:10.1029/2001JA005088.

Dunlop, M. W., D. J. Southwood, K.-H. Glassmeier, and F. M. Neubauer (1988), Analysis of
multipoint magnetometer data, *Adv. Space Res.*, 8, 273, 1988, doi:10.1016/0273-1177(88)90141-x.

Eastwood, J. P., et al. (2008), THEMIS observations of a hot flow anomaly: Solar wind,
magnetosheath, and ground-based measurements, *Geophys. Res. Lett.*, 35, L17S03,
doi:10.1029/2008GL033475.

Ergun, R. E., et al. (2014), The axial double probe and fields signal processing for the MMS
mission, *Space Sci. Rev.*, pp. 1–22, doi:10.1007/s11214-014-0115-x

Fermo, R. L., J. F. Drake and M. Swisdak, (2012). Secondary magnetic islands generated by the
Kelvin-Helmholtz instability in a reconnecting current sheet. *Physical Review Letters*, 108(25),
255005. <https://doi.org/10.1103/PhysRevLett.108.255005>

Gingell, I., Schwartz, S. J., Burgess, D., Johlander, A., Russell, C. T., Burch, J. L., ... Wilder, F.
(2017). MMS observations and hybrid simulations of surface ripples at a marginally quasi-parallel
shock. *Journal of Geophysical Research: Space Physics*, 122, 11,003– 11,017.
<https://doi.org/10.1002/2017JA024538>

Gingell, I., Schwartz, S. J., Eastwood, J. P., Burch, J. L., Ergun, R. E., Fuselier, S., et al.
(2019). Observations of magnetic reconnection in the transition region of quasi-parallel

shocks. *Geophysical Research Letters*, 46, 1177– 1184. <https://doi.org/10.1029/2018GL081804>

Hamrin, M., Gunell, H., Goncharov, O., De Spiegeleer, A., Fuselier, S., Mukherjee, J., et al (2019). Can reconnection be triggered as a solar wind directional discontinuity crosses the bow shock? — A case of asymmetric reconnection. *Journal of Geophysical Research: Space Physics*, 124. <https://doi.org/10.1029/2019JA027006>

Hasegawa, H., Zhang, H., Lin, Y., Sonnerup, B. U. Ö., Schwartz, S. J., Lavraud, B., and Zong, Q.-G. (2012), Magnetic flux rope formation within a magnetosheath hot flow anomaly, *J. Geophys. Res.*, 117, A09214, doi:10.1029/2012JA017920.

Lepping, R. P., et al. (1995), The WIND magnetic field investigation, *Space Sci. Rev.*, 71, 207–229, doi:10.1007/BF00751330.

Lin, Y. (1997), Generation of anomalous flows near the bow shock by its interaction with interplanetary discontinuities, *J. Geophys. Res.*, 102 (A11), 24265– 24281, doi:10.1029/97JA01989.

Lindqvist, P.-A., Olsson, G., Torbert, R. B., King, B., Granoff, M., Rau, G. Needell, et al, S. (2016). The Spin-Plane Double Probe Electric Field Instrument for MMS. *Magnetospheric Multiscale, Space Sci Rev.*, 199, 137–165. doi:10.1007/978-94-024-0861-4_6.

Liu, T. Z., Angelopoulos, V., Hietala, H., and Wilson III, L. B. (2017a), Statistical study of

particle acceleration in the core of foreshock transients, *J. Geophys. Res. Space Physics*, 122, 7197– 7208, doi:10.1002/2017JA024043.

Liu, T. Z., Lu, S., Angelopoulos, V., Hietala, H., and Wilson, L. B. (2017b), Fermi acceleration of electrons inside foreshock transient cores, *J. Geophys. Res. Space Physics*, 122, 9248– 9263, doi:10.1002/2017JA024480.

Liu, T. Z., Angelopoulos, V., and Hietala, H. (2017c), Energetic ion leakage from foreshock transient cores, *J. Geophys. Res. Space Physics*, 122, 7209– 7225, doi:10.1002/2017JA024257.

Liu, T. Z., Lu, S., Angelopoulos, V., Lin, Y., & Wang, X. Y. (2018). Ion acceleration inside foreshock transients. *Journal of Geophysical Research: Space Physics*, 123, 163–178. <https://doi.org/10.1002/2017JA024838>

Liu, T. Z., Angelopoulos, V., and Lu, S. (2019), Relativistic electrons generated at Earth's quasi-parallel bow shock, *Science Advances*, 5, 7, doi:10.1126/sciadv.aaw1368

Lockwood, M. (1991), Flux transfer events at the dayside magnetopause: Transient reconnection or magnetosheath dynamic pressure pulses?, *J. Geophys. Res.*, 96(A4), 5497– 5509, doi:10.1029/90JA02389.

Matsumoto, Y. et al., (2015). Stochastic electron acceleration during spontaneous turbulent reconnection in a strong shock wave. *Science*, 347(6225), pp.974–978. doi:10.1126/science.1260168.

Omidi, N., and D. G. Sibeck, (2007), Formation of hot flow anomalies and solitary shocks, *J. Geophys. Res.*, 112, A01203, doi:10.1029/2006JA011663.

Onsager, T. G., M. F. Thomsen, J. T. Gosling, and S. J. Bame, (1990), Observational test of a hot flow anomaly formation mechanism, *J. Geophys. Res.*, 95(A8), 11967– 11974, doi:10.1029/JA095iA08p11967.

Pollock, C., et al. (2016), Fast plasma investigation for magnetospheric multiscale, *Space Sci. Rev.*, pp. 1–76, doi:10.1007/s11214-016-0245-4.

Russell, C. T. & R. C. Elphic, (1979). Observation of magnetic flux ropes in the Venus ionosphere. *Nature*, 279(5714), pp.616–618. doi:10.1038/279616a0.

Russell, C. T., et al. (2016), The magnetospheric multiscale magnetometers, *Space Sci.Rev.*, 199, 189–256, doi:10.1007/s11214-014-0057-3

Schwartz, S. J. (1998). Shock and discontinuity normals, mach numbers, and related parameters. *ISSI Scientific Reports Series*, 1, 249–270, ISSI/ESA, Noordwijk, Netherlands.

Schwartz, S. J., et al. (1985), An active current sheet in the solar wind, *Nature*, 318, 269–271, doi:10.1038/318269a0.

Schwartz, S. J., Paschmann, G., Sckopke, N., Bauer, T. M., Dunlop, M., Fazakerley, A. N., and Thomsen, M. F. (2000), Conditions for the formation of hot flow anomalies at Earth's bow shock, *J. Geophys. Res.*, 105(A6), 12639– 12650, doi:10.1029/1999JA000320.

Shen, C., X. Li, M. Dunlop, Q. Q. Shi, Z. X. Liu, E. Lucek, and Z. Q. Chen (2007), Magnetic field rotation analysis and the applications, *Journal of Geophysical Research: Space Physics*, 112(A6), doi:10.1029/2005JA011584.

Shi, Q. Q., C. Shen, Z. Y. Pu, M. W. Dunlop, Q.-G. Zong, H. Zhang, C. J. Xiao, Z. X. Liu, and A. Balogh (2005). Dimensional analysis of observed structures using multipoint magnetic field measurements: Application to Cluster. *Geophysical Research Letters*, 32, L12105. doi:10.1029/2005GL022454

Shi, Q. Q., A. M. Tian, S. C. Bai, H. Hasegawa, A. W. Degeling, Z. Y. Pu, M. Dunlop, R. L. Guo, S. T. Yao, Q.-G. Zong, Y. Wei, X.-Z. Zhou, S. Y. Fu, and Z. Q. Liu (2019), Dimensionality, Coordinate System and Reference Frame for Analysis of In-Situ Space Plasma and Field Data, *Space Sci. Rev.*, 215, 4. doi:10.1007/s11214-019-0601-2

Sibeck, D. G. (1990), A model for the transient magnetospheric response to sudden solar wind dynamic pressure variations, *J. Geophys. Res.*, 95(A4), 3755– 3771, doi:10.1029/JA095iA04p03755.

Slavin, J. A., and R. E. Holzer (1981). Solar wind flow about the terrestrial planets. I - Modeling bow shock position and shape. *Journal of Geophysical Research*, 86, 11,401–11,418. doi:10.1029/JA086iA13p11401.

Slavin, J. A., R. P. Lepping, J. Gjerloev, D. H. Fairfield, M. Hesse, C. J. Owen, M. B. Moldwin, T. Nagai, A. Ieda, and T. Mukai (2003), Geotail observations of magnetic flux ropes in the plasma sheet, *Journal of Geophysical Research: Space Physics*, 108(A1), SMP 10-11-SMP 10-18, doi:10.1029/2002JA009557.

Smith, C. W., J. L'Heureux, N. F. Ness, M. H. Acuña, L. F. Burlaga, and J. Scheifele (1998), The ACE magnetic fields experiment, *Space Sci. Rev.*, 86, 613–632, doi:10.1023/A:1005092216668.

Sonnerup, B. U. Ö., and L. J. Cahill, (1967). Magnetopause structure and attitude from Explorer 12 observations. *Journal of Geophysical Research*, 72(1), 171. doi:10.1029/jz072i001p00171

Sonnerup, B. U. Ö., I. Papamastorakis, G. Paschmann, and H. Lühr, (1987), Magnetopause properties from AMPTE/IRM observations of the convection electric field: Method development, *J. Geophys. Res.*, 92(A11), 12137– 12159, doi:10.1029/JA092iA11p12137.

Sun, W. J., J. A. Slavin, A. M. Tian, S. C. Bai, G. K. Poh, M. Akhavan-Tafti et al. (2019). MMS study of the structure of ion-scale flux ropes in the Earth's cross-tail current sheet. *Geophysical Research Letters*, 46. doi:10.1029/2019GL083301

Thomsen, M. F., J. T. Gosling, S. J. Bame, K. B. Quest, C. T. Russell and S. A. Fuselier (1988), On the origin of hot diamagnetic cavities near the Earth's bow shock, *J. Geophys. Res.*, 93(A10), 11311– 11325, doi:10.1029/JA093iA10p11311.

Thomsen, M. F., V. A. Thomas, D. Winske, J. T. Gosling, M. H. Farris, and C. T. Russell (1993), Observational test of hot flow anomaly formation by the interaction of a magnetic discontinuity with the bow shock, *J. Geophys. Res.*, 98(A9), 15,319–15,330, doi:10.1029/93JA00792

Turner, D. L., Wilson, L. B., Liu, T. Z., Cohen, I. J., Schwartz, S. J., Osmane, A., & Burch, J. L. (2018). Autogenous and efficient acceleration of energetic ions upstream of Earth's bow shock. *Nature*, 561(7722), 206–210. <https://doi.org/10.1038/s41586-018-0472-9>.

Wang, S., Q.-G. Zong, and H. Zhang (2013a), Cluster observations of hot flow anomalies with large flow deflections: 1. Velocity deflections, *J. Geophys. Res.*, 118, 732–743, doi:10.1002/jgra.50100.

Wang, S., Q.-G. Zong, and H. Zhang (2013b), Cluster observations of hot flow anomalies with large flow deflections: 2. Bow shock geometry at HFA edges, *J. Geophys. Res.*, 118, 418–433, doi:10.1029/2012JA018204.

Wang, S., Q.-G. Zong, and H. Zhang (2013c), Hot flow anomaly formation and evolution: Cluster observations, *J. Geophys. Res.*, 118, 4360–4380, doi:10.1002/jgra.50424.

Wang, S., Chen, L.-J., Bessho, N., Hesse, M., Wilson, L. B., Giles, B., et al. (2019). Observational evidence of magnetic reconnection in the terrestrial bow shock transition region. *Geophysical Research Letters*, 46, 562–570. <https://doi.org/10.1029/2018GL080944>.

Wilson, L. B. III, D. G. Sibeck, D. L. Turner, A. Osmane, D. Caprioli, and V. Angelopoulos (2016),

Relativistic electrons produced by foreshock disturbances observed upstream of Earth's bow shock, *Phys. Rev. Lett.*, 117, 215101, doi:10.1103/PhysRevLett.117.215101.

Zhang, H., et al. (2010), Time history of events and macroscale interactions during substorms observations of a series of hot flow anomaly events, *J. Geophys. Res.*, 115, A12235, doi:10.1029/2009JA015180.

Zhao, L. L., Q.-G. Zong, H. Zhang, and S. Wang (2015), Case and statistical study on evolution of hot flow anomalies, *J. Geophys. Res. Space Physics*, 120, doi:10.1002/2014JA020862.

Zhao, L. L., H. Zhang, and Q. G. Zong (2017), A statistical study on hot flow anomaly current sheets, *J. Geophys. Res. Space Physics*, 122, 235–248, doi:10.1002/2016JA023319.

Zong, Q.-G., et al. (2004), Cluster observations of earthward flowing plasmoid in the tail, *Geophys. Res. Lett.*, 31, L18803, doi:10.1029/2004GL020692.

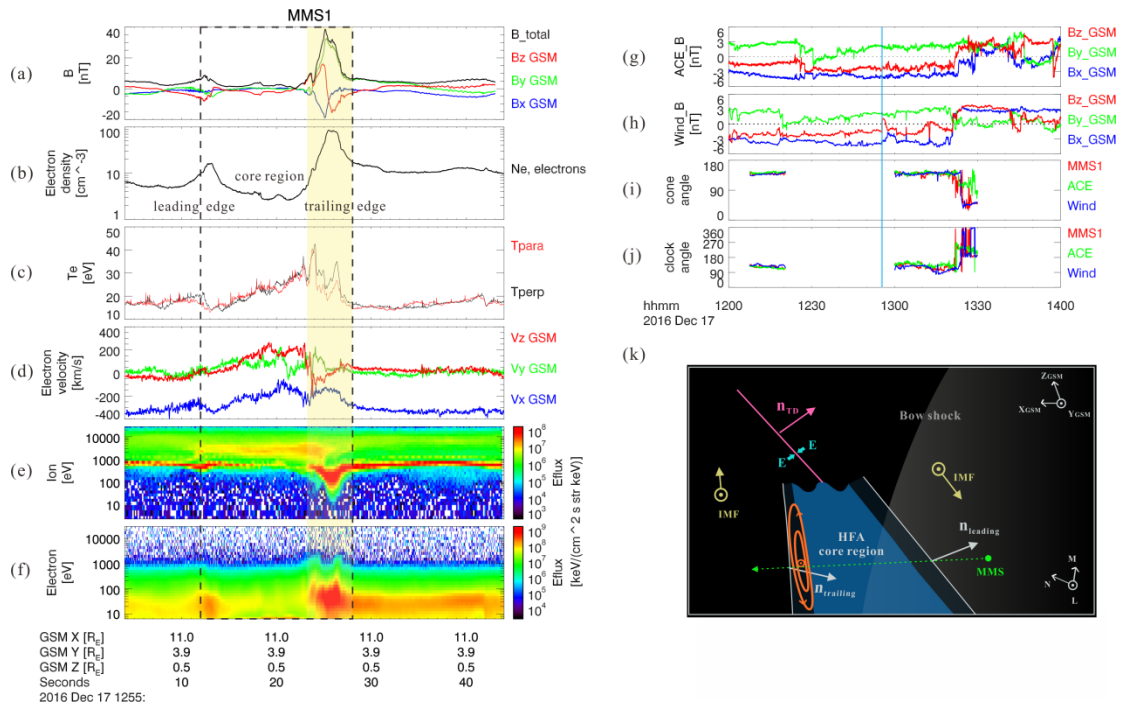


Figure 1: An overview plot of MMS1 observation of the flux rope inside the HFA. The blue/green/red line for X/Y/Z component in GSM coordinate. From top to bottom: (a) magnetic field; (b) electron number density; (c) electron parallel (red line) and perpendicular (black line) temperature; (d) electron velocity; (e) omni-directional ion energy flux; (f) omni-directional electron energy flux; (g) magnetic field observed by ACE and shifted to the MMS location; (h) magnetic field observed by Wind and Shifted to the MMS location; (i) IMF cone angle observed by ACE, Wind and MMS1; (j) IMF clock angle of interplanetary magnetic field (IMF) observed by ACE, Wind and MMS1; (k) illustration of the HFA and the relative trajectory of MMS. To better illustrate the flux rope, HFA and bow shock, X and Z are not perpendicular to each other. M and N are not perpendicular to each other too. The normal directions of both edges are not perpendicular to the edges. The normal direction of the TD is not perpendicular to the TD in panel k. The HFA is marked by the black dashed box and the flux rope is marked by the yellow shaded region. The time interval of Figures 1a-f is marked by the blue shaded region in Figures 1g-j.

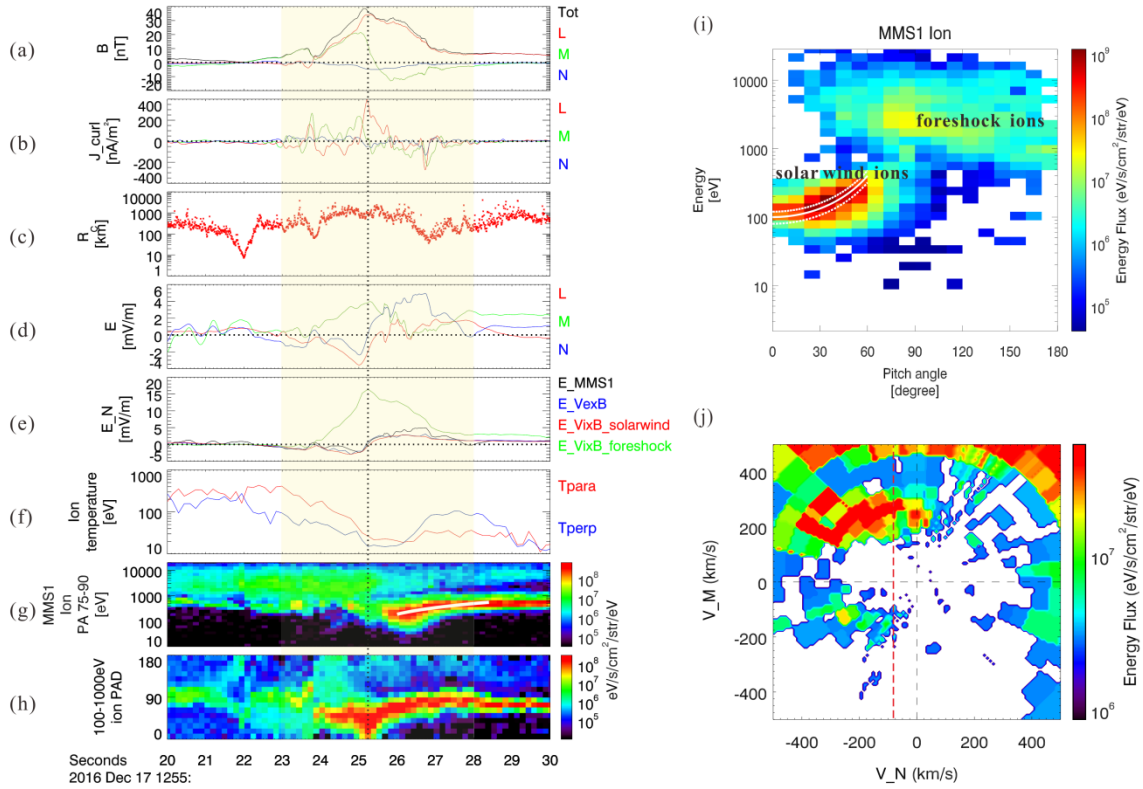


Figure 2: MMS observation of the flux rope in L-M-N coordinate from 12:55:23 to 12:55:28 UT marked by the yellow shade region. The blue/green/red line represents the L/M/N component. From top to bottom: (a) magnetic field; (b) current density; (c) the radius of magnetic curvature R_c ; (d) electric field; (e) N component of the electric field with the black from the MMS1 measurements, red from the foreshock ion motion, green from the solar wind ion motion and blue from the electron motion; (f) perpendicular and parallel temperature of the solar wind ions; (g) perpendicular ion energy flux; (h) 100-1000 eV ion pitch angle distribution; (i) the ion distribution ($\text{eV/s/cm}^2/\text{str/eV}$) displays as a function of energy and pitch angle at 12:55:25.24 UT (vertical dashed line in Figures 2a-g); (j) the ion distribution ($\text{eV/s/cm}^2/\text{str/eV}$) in the M-N plane at 12:55:25.24 UT. The white solid line in Figure 2f is the solar wind energy decrease as $1.7 \text{ mV/m} \cdot 133.56 \text{ km}$ in the de Hoffmann Teller frame ($V_{\text{HT}}=232.5 \times [-0.96, 0.28, 0.07] \text{ km/s}$) and transformed it back to the spacecraft frame. The curved lines in the Figure 2h, given by $\theta = \cos^{-1} [(E_{//}/E)^{1/2}]$, show the contour

line of parallel energy $E_{\parallel}=80$ eV (dashed line), 100 eV (solid line), and 120 eV (dashed line). The red dashed line is the velocity ($V_N=-89.04$ km/s) of the trailing edge of the HFA base on the timing analysis.

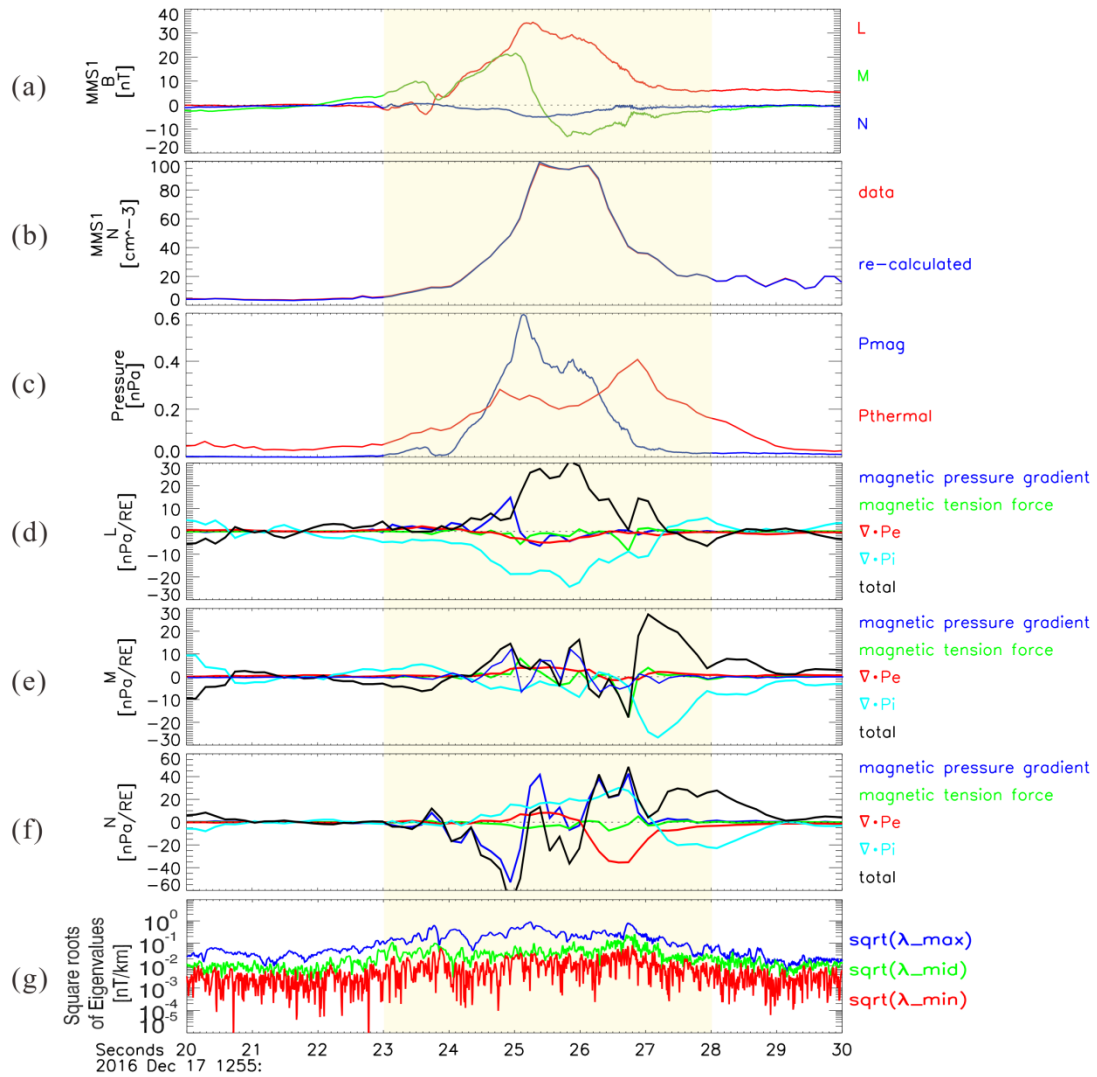
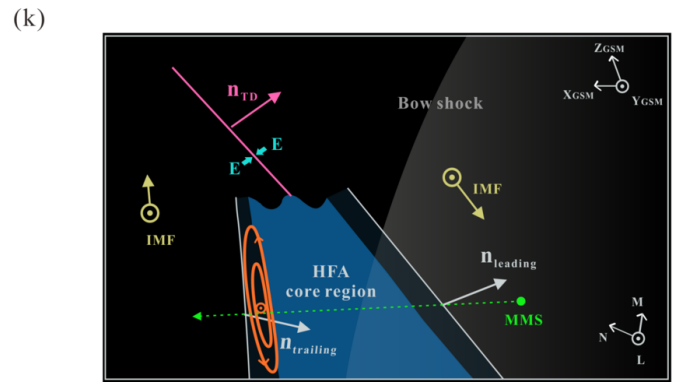
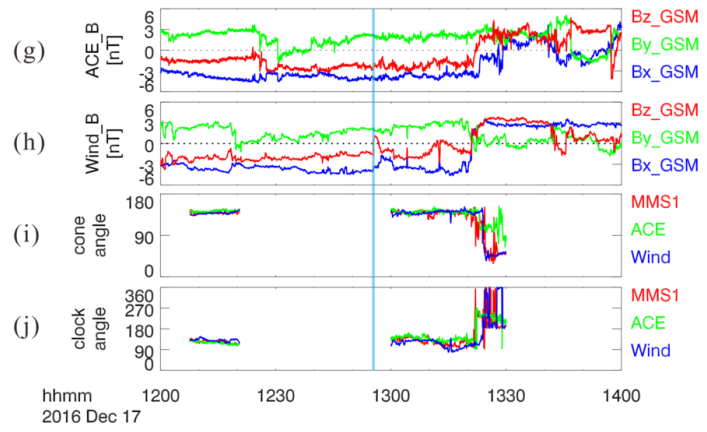
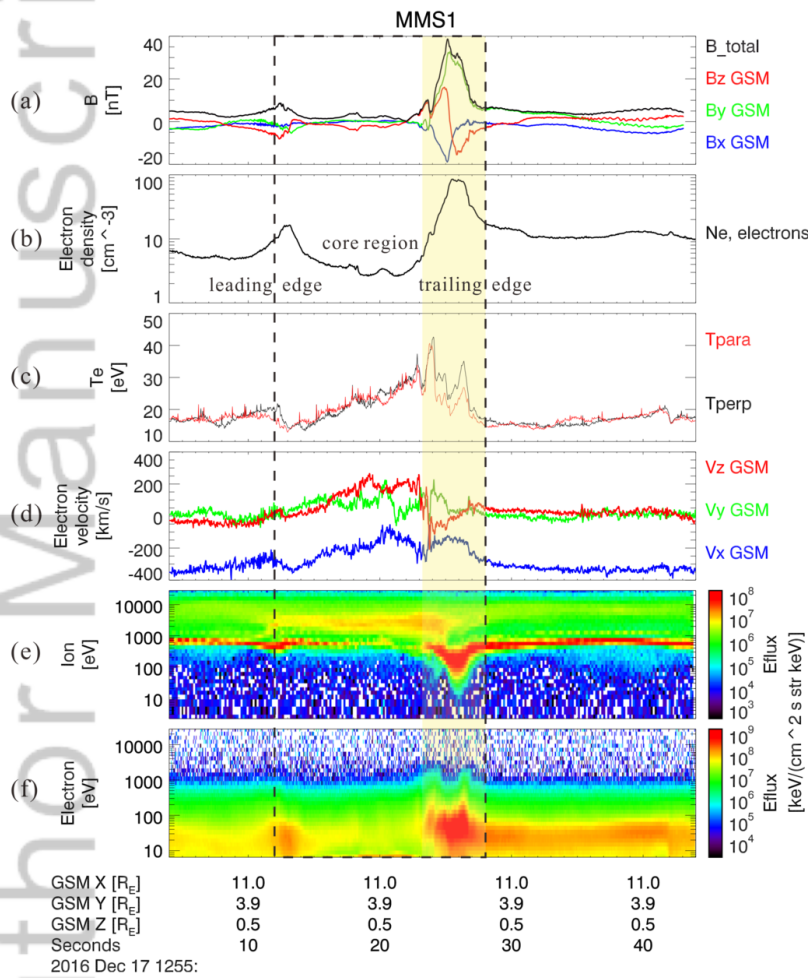
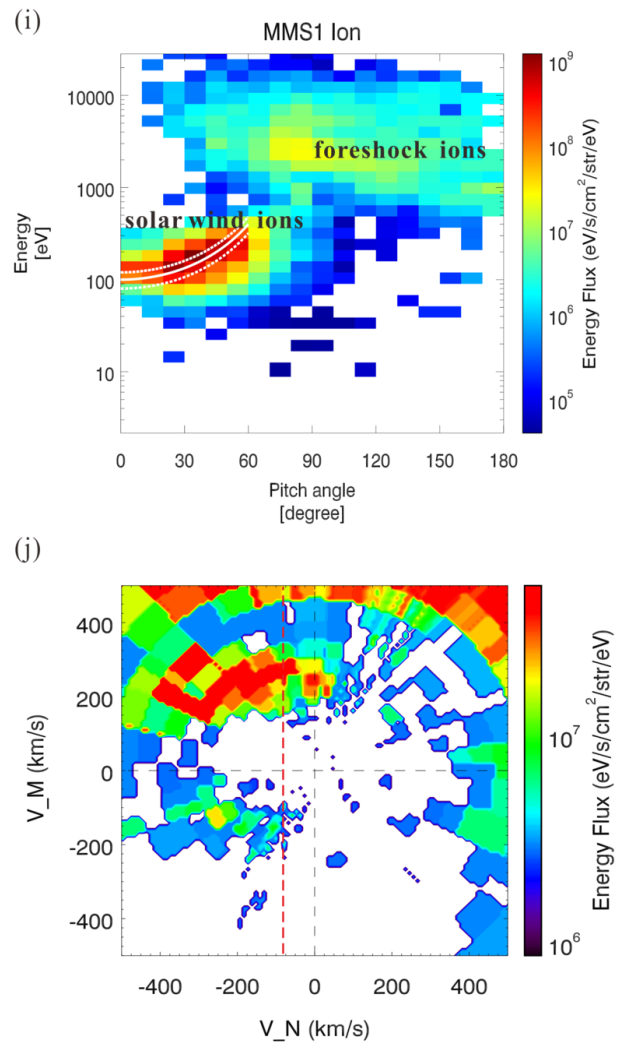
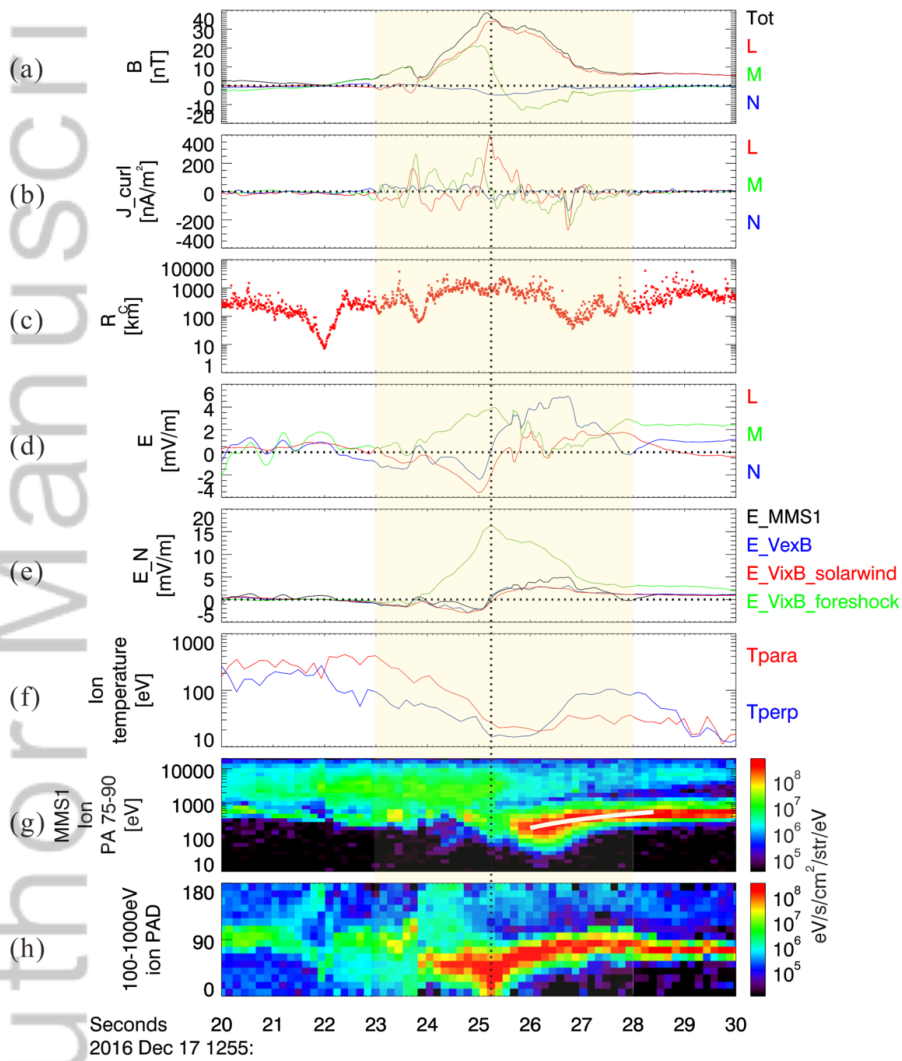


Figure 3: (a) Magnetic field in L-M-N coordinates; (b) ion density from MMS1 FPI data shown in red and from the re-calculated MMS1 FPI data shown in blue; (c) magnetic pressure shown in blue and thermal pressure shown in red; (d) L component of the force analysis; (e) M component of the force analysis; (f) N component of the force analysis with the black being the summation of different force contribution, the blue being the magnetic pressure gradient force, the green being the magnetic tension force, the cyan being the ion pressure gradient force and red being the electron

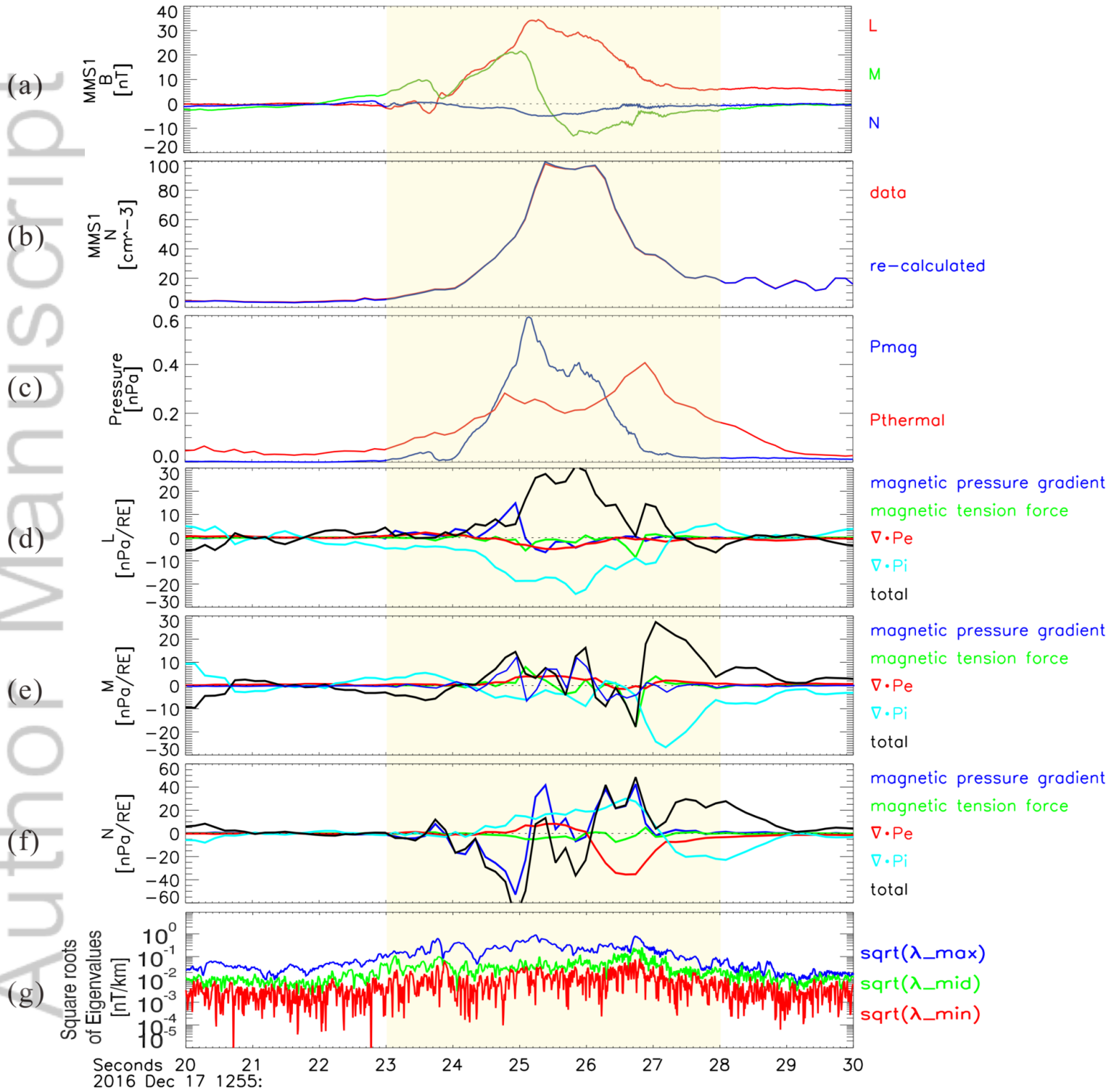
pressure gradient force; (g) eigenvalues resulted from MDD, $\sqrt{\lambda_{max}}$ is in blue,
 $\sqrt{\lambda_{mid}}$ in green, $\sqrt{\lambda_{min}}$ in red; The flux rope is marked by the yellow shaded region.



2019GL085933-f01-z.png



2019GL085933-f02-z-.png



2019GL085933-f03-z.png